Articles

Analysis of the Kinetic and Redox Properties of the NADH Peroxidase R303M Mutant: Correlation with the Crystal Structure†,‡

Edward J. Crane, III,§,|| Joanne I. Yeh,⊥ James Luba,§ and Al Claiborne*,§

Department of Biochemistry, Wake Forest University Medical Center, Winston-Salem, North Carolina 27157, and Department of Molecular Biology, Cell Biology, and Biochemistry, Brown University, Providence, Rhode Island 02912

Received March 10, 2000; Revised Manuscript Received June 26, 2000

ABSTRACT: The crystal structure of the flavoprotein NADH peroxidase shows that the Arg303 side chain forms a hydrogen bond with the active-site His10 imidazole and is therefore likely to influence the catalytic mechanism. Dithionite titration of an R303M mutant [E(FAD, Cys42-sulfenic acid)] yields a two-electron reduced intermediate (EH_2) with enhanced flavin fluorescence and almost no charge-transfer absorbance at pH 7.0; the pK_a for the nascent Cys42-SH is increased by over 3.5 units in comparison with the wild-type EH_2 pK_a of ≤4.5. NADH titration of the mutant peroxidase yields the same EH_2 intermediate, but in contrast to the behavior of wild-type enzyme, this species can be reduced directly to an EH_4·NAD^+ complex. Kinetic analyses demonstrate that the R303M mutant is severely compromised, although active, with $k_{cat} = 3\ s^{-1}$ at pH 7.0, 5 °C; enzyme-monitored turnover results indicate that the steady-state consists predominantly of an E-$FADH_2$·NAD^+ species. When the oxidized mutant is reacted anaerobically with 0.9 equiv of NADH/FAD, a clearly biphasic pattern is observed at 450 nm; relatively rapid flavin reduction is followed by reoxidation at 2.6−2.7 s^{-1} (∼k_{cat}). Thus replacement of Arg303 with Met leads to an altered peroxidase form in which the rate-limiting step in turnover is the intramolecular transfer of electrons from $FADH_2$ → Cys42-SOH. The crystal structure of the R303M peroxidase has been refined at 2.45 Å resolution. In addition to eliminating the Arg303 interactions with His10 and Glu14, the mutant exhibits a significant change in the conformation of the Cys42-SOH side chain relative to FAD and His10 in particular. These and other results provide a detailed understanding of Arg303 and its role in the structure and mechanism of this unique flavoprotein peroxidase.

Although over 40 years have passed since its original identification by Dolin (*1*), the flavoprotein NADH peroxidase (Npx;[1] NADH + H^+ + H_2O_2 → NAD^+ + $2H_2O$) remains the only known FAD- (or FMN-) dependent peroxidase (*2*, *3*). Crystal structures have been reported for the inactive Cys42-SO_3H derivative and its complex with NADH (*4*, *5*) and for several active-site mutants including the C42S, C42A, and S41C proteins (*6*, *7*) as well as the L40C mutant, which forms an active-site disulfide between Cys40-SH and the native Cys42-SOH redox center. Mande et al. (*6*) were the first to observe a hydrogen bond between Arg303 $N_{\eta 1}$ and His10 $N_{\delta 1}$; as a result, it was concluded that His10 is very likely to remain unprotonated throughout the catalytic cycle. Subsequent studies with His10 mutants (*8*) have supported this conclusion. While the neutral His10 $N_{\epsilon 2}$−H tautomer stabilized by the interaction with Arg303 plays important roles in the stabilization of both the Cys42-SOH redox center in the resting enzyme and the transition state for peroxide reduction by Cys42-S^-, it is not an essential acid−base catalyst. Somewhat surprisingly, however, the replacement of Arg303 with Met in an HHAA peroxidase mutant retaining His10 and His23 (*9*) had no significant effect on the ^{13}C His NMR spectrum of the labeled protein over the pH range 6.0−8.0. As also described by Mande et al. (*6*), Arg303 forms a salt bridge with Glu14; Stehle et al. (*4*) originally identified this interaction as a component of the "domain zipper" linking the N-terminal FAD-binding and

† This work was supported by National Institutes of Health Grant GM-35394. E.J.C. and J.I.Y. were the recipients of National Research Service Awards GM-16274 and DK-09568, respectively. J.I.Y. also acknowledges the financial support of Dr. Wim G. J. Hol (Department of Biological Structure, University of Washington, Seattle, WA).

‡ Coordinates have been deposited with the Protein Data Bank under the file name 1F8W.

* To whom correspondence should be addressed. Phone: (336) 716-3914. Fax: (336) 716-7671. URL: http://invader.bgsm.wfu.edu/.

§ Wake Forest University Medical Center.

|| Present address: Department of Chemistry, Salisbury State University, Salisbury, MD 21801.

⊥ Brown University.

[1] Abbreviations: Npx, NADH peroxidase; Cys-SOH and Cyo, cysteine-sulfenic acid; EH_2, two-electron reduced enzyme (FAD, Cys-SH); Nox, NADH oxidase; AcPyADH, 3-acetylpyridine adenine dinucleotide, reduced; $E'°$, midpoint oxidation−reduction potential at pH 7.0; EH_4, four-electron reduced enzyme ($FADH_2$, Cys-SH); HEPES, *N*-[2-hydroxyethyl]piperazine-*N*′-[2-ethanesulfonic acid]; CHES, 2-[*N*-cyclohexylamino]ethanesulfonic acid; Cys-SO_2H, Cys-sulfinic acid; Cys-SO_3H, Cys-sulfonic acid; EH_2', two-electron reduced enzyme ($FADH_2$, Cys-SOH); NADD, (4*S*)-[4-^{2}H]NADH; EHR, two-electron reduced, monoalkylated enzyme; GR, glutathione reductase.

10.1021/bi000553m CCC: $19.00
Published on Web 08/02/2000

Central domains. There is also an interesting interaction observed originally in the Cys42 mutant structures between Arg303 $N_{\eta 1}$ and the aromatic ring of Tyr60, which was interpreted as an example of hydrogen bonding between the Arg303 primary amino group and the π electrons of the benzene ring.

More recently, we have described the active-site structures of the native Cys42-SOH forms of both wild-type and H10Q Npx at 2.1 and 2.4 Å, respectively (*3*). While the presence of a hydrogen bond between Arg303 and His10 is clearly indicated in the wild-type structure, the conformation of the Arg303 side chain has changed from that seen in the Cys42 mutants such that Arg303 N_{ϵ}, not $N_{\eta 1}$, interacts (3.0 Å) with His10 $N_{\delta 1}$. In the H10Q mutant, the guanidinium moiety of Arg303 is completely flipped relative to the wild-type conformation. In comparing the Arg303 conformations of the Cys42-SOH and C42S forms of Npx, it appeared that the observed side chain movement could be of catalytic significance, especially since the Ser42 side chain is an isosteric equivalent of the Cys42-SH present in the Npx EH_2 intermediate. In addition, the refined 2.5 Å crystal structure[2] of the *Streptococcus pyogenes* NADH oxidase C44S mutant (Nox; $2NADH + 2H^+ + O_2 \rightarrow 2NAD^+ + 2H_2O$), a close structural and mechanistic homologue of Npx, demonstrates that Arg303 of the peroxidase is replaced with Val314; this Val residue is conserved in all five known Nox sequences as either Val or Leu. This observation suggests that Arg303 may play a critical role in determining peroxidase versus oxidase function as well. In this report we present a detailed analysis of the kinetic and redox properties of the Npx R303M mutant, and we also describe the crystal structure for this protein, refined at 2.45 Å resolution.

EXPERIMENTAL PROCEDURES

Materials and General Methods. NADH was purchased from Boehringer Mannheim, and AcPyADH and phenosafranin were from Sigma. (4*S*)-[4-^{1}H]- and (4*S*)-[4-^{2}H]NADH were prepared as described previously (*10*); all other chemicals were purchased from sources given earlier (*11*) and were of the best grades available. NADH peroxidase activity was routinely measured using the established procedure (*12*). Spectral titrations were carried out with Hewlett-Packard model 8452A and Beckman DU 7500 diode-array spectrophotometers and with an SLM AB2 spectrofluorimeter; procedures for anaerobiosis have been described (*11*). E'° for the R303M peroxidase EH_2/EH_4 redox couple was determined by dithionite titration in the presence of the reference dye phenosafranin ($E'^{\circ} = -252$ mV; ref *13*), using methyl viologen at low concentration to ensure rapid equilibration of reducing equivalents (*11*).

Stopped-Flow Measurements. The Applied Photophysics DX.17 MV stopped-flow spectrophotometer, equipped with a photodiode-array detector and Acorn 32 bit RISC-processor workstation (*14*, *15*), was thermostated at 5 °C and used (1) to determine the steady-state kinetic parameters for R303M Npx from initial rates of NADH and AcPyADH oxidation, (2) to perform spectral and kinetic enzyme-monitored turnover analyses, including the primary deuterium kinetic isotope effects on both the approach to steady state and turnover, (3) to analyze the kinetic and spectral events during reduction to the EH_2 and $EH_4{\cdot}NAD^+$ forms and on oxidation of EH_2 with H_2O_2, and (4) to determine the pK_a for Cys42-SH in the R303M Npx EH_2 form. These analyses involved single-wavelength absorbance (NADH, AcPyADH, or enzyme), fluorescence emission at a fixed excitation wavelength (NADH or enzyme), and diode-array measurements (enzyme), as described previously. A standard buffer of 50 mM potassium phosphate, 0.1 M potassium acetate, pH 7.0, plus 0.5 mM EDTA was used in all spectral titrations and routine stopped-flow experiments. Steady-state kinetic parameters for NADH and H_2O_2 at pH 7.0, 5 °C, were determined by measuring initial rates of NADH oxidation (*10*) when buffered enzyme was mixed in the stopped-flow spectrophotometer with substrate solutions (final concentrations of 1−77 μM NADH, 1−40 mM H_2O_2, and 25 nM Npx). At [NADH]s $\leq$20 μM oxidation was monitored by the decrease in fluorescence ($\lambda^{EX} = 340$ nm), using an emission cutoff filter which allowed transmission of light at $\lambda > 385$ nm; for each set of measurements a standard curve was constructed to allow the conversion of fluorescence units to [NADH]. These standard curves also demonstrated that fluorescence intensity was linearly proportional to [NADH] over the range 0−20 μM (A340 = 0−0.12). At [NADH]s > 20 μM initial rates were measured from the decrease in A340. In all cases, the initial velocities reported represent the averages from four individual traces and are corrected for Npx-catalyzed NADH oxidation in the absence of H_2O_2. Kinetic parameters were determined using ENZFITTER, as previously described (*10*). The pK_a for Cys42-SH in the R303M Npx EH_2 form was determined at 5 °C by mixing EH_2 (23 μM before mixing, in 7.5 mM phosphate, pH 7.0) with 0.1 M potassium phosphate, pH 7.0; 0.1 M HEPES, pH 7.5, 7.8, and 8.3; and 0.1 M CHES, pH 8.7 and 9.0, in the stopped-flow spectrophotometer and measuring the amplitude of the absorbance increase at 560 nm. Final pH values were measured in controls at 25 °C and corrected for the change in temperature. All buffers contained 0.5 mM EDTA. As required, the stopped-flow system was prepared for anaerobic work as previously described (*14*).

Stopped-flow analyses of enzyme-monitored turnover (*16*) and $E \rightarrow EH_2$ reduction consisted of both single-wavelength (primarily 450 and 660 nm) and diode-array data sets, and the Pro-Kineticist (Pro-K; Applied Photophysics) software was used for global analysis of these data, including calculations of intermediate spectra (*14*). The reductions of E and $EH_2 \rightarrow EH_4{\cdot}NAD^+$ were monitored only by diode-array detection, and in these cases, rate constants were estimated by analyzing the entire data set at selected wavelengths of 450 and 750 nm. For calculations of intermediate spectra sequential mechanisms of the type A $\rightarrow$ B $\rightarrow$ C, etc., were employed, where species A was represented by the starting spectrum of the free E (or EH_2, respectively) form of R303M Npx. In analyzing the specific reaction of E with 5 equiv of (4*S*)-[4-^{2}H]NADH, however, the dead-time spectrum corresponding to A was also calculated. In this case, 400 absorbance spectra were collected in a linear time base from 3.8 ms to 2 s.

Protein Purification and Crystallization. The R303M mutation was generated in the plasmid pNPR4 (*17*), and the final pR303M expression plasmid was checked by both

[2] T. C. Mallett, H. Sakai, D. Parsonage, A. Claiborne, and T. Tsukihara, manuscript in preparation.

Table 1: Data Collection and Refinement Statistics for R303M Npx

space group	$I4_122$
cell parameters (Å)	$a = b = 155.10$; $c = 189.29$
resolution range (Å)	20−2.45
resolution range in refinement (Å)	8.0−2.45
total number of reflections	60 231
no. of independent reflections	36 615
completeness (%)	85.8
completeness at highest resolution shell (%)	70.9 (2.45−2.56)
avg *B* factor (Å^2)	39.1
no. of unique reflections > 3σ	26 310
R_{merge}[a] (%)	4.8
R_{merge} at highest resolution shell (%)	36.3 (2.45−2.56)
$R_{crystallographic}$[a] (%)	19.6
R_{free}[b] (%)	23.4
rms bond length (Å)	0.010
rms bond angle (deg)	2.6
rms coordinate error (Å)	0.25
no. of protein and FAD atoms	3541
no. of water molecules	131

[a] All *R* factors are defined as $R = (\Sigma|F_o - F_c|)/\Sigma F_o$, where F_o is the observed structure factor amplitude and F_c is the calculated structure factor amplitude. [b] R_{free} is calculated with 10% of the data that are not included in the refinement.

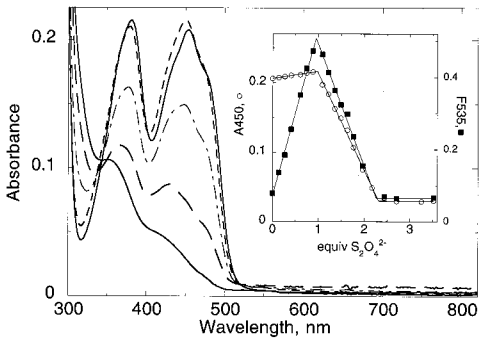

FIGURE 1: Anaerobic dithionite titration of the R303M peroxidase. Enzyme was initially treated with 1 equiv of H_2O_2/FAD to reoxidize any EH_2 and was then dialyzed by ultrafiltration. The anaerobic cuvette contained 19.5 μM enzyme (FAD) in 50 mM phosphate, pH 7.0, with 0.5 mM EDTA. Spectra shown were measured approximately 1 h after the respective addition of reductant, to allow complete equilibration of reducing equivalents. In order of decreasing A380, these correspond to oxidized enzyme (—) and enzyme after addition of 0.88 (- - -), 1.49 (- · -), 1.96 (— — —), and 2.7 (—) equiv of dithionite/FAD. Inset: Changes in A450 and in fluorescence emission at 535 nm (λ^{EX} = 450 nm) versus added dithionite. The end points correspond to 0.96 and 2.3 equiv of dithionite/FAD.

sequence and restriction analysis. The mutant protein was expressed and purified from *Escherichia coli* JM109(DE3) using the procedure developed for recombinant wild-type Npx; crystals of R303M Npx were obtained by the vapor diffusion method under ambient conditions, using solutions containing 2−8% PEG 400, 1.6−1.9 M $(NH_4)_2SO_4$, and 0.1 M sodium HEPES, pH 7.2, with protein concentrations of 7.5−10 mg/mL. Large single, yellow prisms were seen after 3−5 days, and these continued to grow for about one more week. At this stage, crystals were either prepared directly for data collection or stored under argon to limit exposure to oxygen, thus stabilizing Cys42-SOH against oxidation to the inactive Cys42-SO_2H/-SO_3H forms (*18*). Crystals were frozen at 110 K using 30% ethylene glycol as a cryoprotectant; flash-dipping the crystal into artificial mother liquor containing ethylene glycol, then freezing it directly under the nitrogen cold stream, resulted in a successful freezing protocol. R303M Npx crystallized in space group $I4_122$ with one molecule per asymmetric unit.

Data Collection and Refinement. Synchrotron data were collected from a single crystal at Stanford Synchrotron Research Laboratory beamline 7-1; crystal decay was virtually eliminated under the cryogenic conditions employed, as indicated by the image scale factors used during processing. Data were processed in DENZO and scaled in SCALEPACK (*19*); data statistics, cell dimensions, and resolution for the R303M Npx crystals are given in Table 1. The refinement protocol used for the R303M Npx structure was essentially identical to that employed for the H10Q and H10A mutants;[3] the starting model in each case was the 2.8 Å native Cys42-SOH structure of wild-type Npx.

RESULTS

Purification and Spectral Properties. The expression and purification protocol adapted from that developed for recombinant wild-type Npx (*17*) routinely yields 110−120 mg of pure R303M enzyme from 5 L of *E. coli* cultures. As with the wild-type and His10 mutant (*8*) proteins, the fluorescence of the tightly bound FAD is strongly quenched in R303M Npx. The visible absorption spectra of the recombinant wild-type (λ_{max} = 380, 450 nm; ϵ450 = 10 900 M^{-1} cm^{-1}) and R303M mutant (λ_{max} = 380, 453 nm; ϵ453 = 10 600 M^{-1} cm^{-1}) Npxs are very similar; the absorbance ratio at 280 and 450 nm for both enzymes is 7.8. There is no obvious indication from the visible absorbance spectrum that R303M Npx purifies as a mixture of E and EH_2 forms, as was observed with both wild-type and H10Q proteins, nor does the R303M mutant as purified exhibit the enhanced long-wavelength absorbance band attributed to Cys42-SOH → FAD charge-transfer in the oxidized His10 mutants.

Reductive Titrations. Anaerobic dithionite titration of the R303M mutant at pH 7.0 proceeds in two distinct phases, consistent with the presence of functional Cys42-SOH and FAD redox centers (Figure 1). Surprisingly, however, completion of the first phase with 1 equiv of dithionite/FAD does not give rise to the strong EH_2 charge-transfer band (Cys42-S^- → FAD; $\lambda_{max} \sim$ 540 nm) seen with wild-type and His10 mutant Npxs. There are small but significant changes in the 380 and 450 nm absorbance maxima, but these appear to represent a simple perturbation of the flavin environment on reduction of Cys42-SOH → Cys42-SH rather than the altered electronic state associated with a charge-transfer interaction. Another very significant difference in the behavior of R303M Npx during the first phase of this titration concerns the very slow intramolecular transfer of reducing equivalents within the EH_2' intermediate observed transiently on each addition of dithionite. This process, which was followed as a slow reappearance of the starting A450, requires ~1 h for completion under stringent anaerobic conditions at pH 7.0, 25 °C. In all other Npx forms studied to date (*7*, *8*, *17*), the direct reduction of E → EH_2 has been observed in spectral titrations with dithionite or NADH.

Another surprising observation was made when the dithionite titration described above was followed by fluorescence (λ^{EX} = 450 nm, λ^{EM} = 535 nm), as shown in Figure

[3] J. I. Yeh, D. Parsonage, and A. Claiborne, manuscript in preparation.

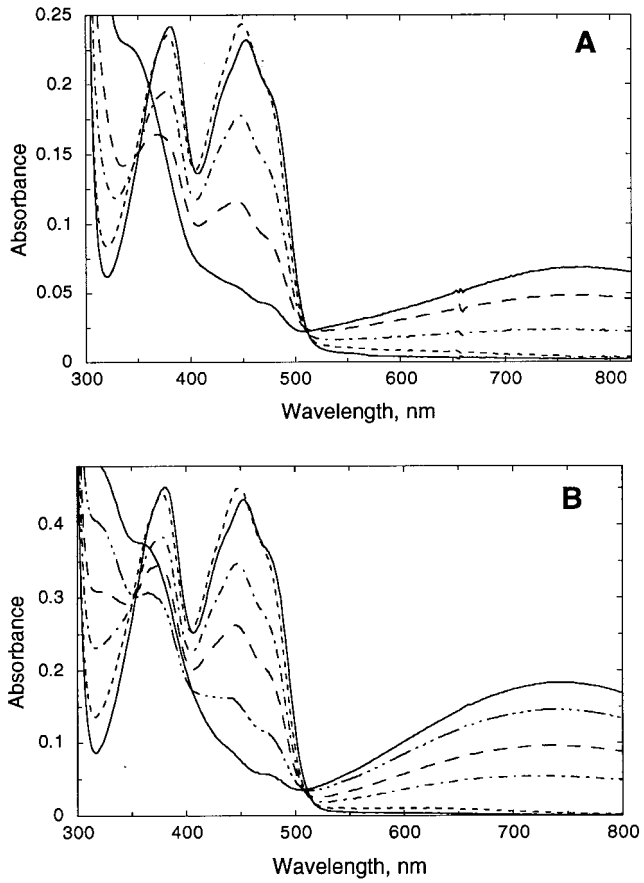

FIGURE 2: Anaerobic titrations of R303M peroxidase with NADH and AcPyADH. (A) In order of increasing A765, the spectra shown correspond to oxidized enzyme [(—) 21.6 μM, treated as described in Figure 1] and enzyme after addition of 0.9 (- - -), 1.42 (- · -), 1.85 (— — —), and 3.27 (—) equiv of NADH/FAD. (B) In order of increasing A740, spectra correspond to oxidized enzyme [(—) 40.6 μM, treated as described above] and enzyme after addition of 0.84 (- - -), 1.19 (- · -), 1.39 (— — —), 1.67 (— · · · —), and 2.4 (—) equiv of AcPyADH/FAD. The oxygen-scrubbing system consisting of protocatechuate dioxygenase and protocatechuic acid was added anaerobically prior to each titration.

1. While the oxidized enzyme exhibits only 1−2% of the fluorescence intensity of free FAD at the same concentration, reduction of E → EH_2 is associated with a distinctive 6−7-fold increase in fluorescence. The enhanced quantum yield for the EH_2 form of R303M Npx is similar to that reported for the oxidized C42S, C42A, and L40C mutants (*7*, *11*). There is no evidence for any kinetic or thermodynamic stabilization of flavin semiquinone during either phase of the titration, and addition of 1.3 equiv of dithionite/FAD to the R303M EH_2 intermediate leads directly to the fully reduced EH_4 species. The distinct absorbance maximum at 355 nm is consistent with stabilization of the N(1)-anionic form of $FADH_2$, as seen with the wild-type enzyme (*20*). As expected, the reduction of the R303M Npx EH_2 form to EH_4 (FAD → $FADH_2$) in the second phase of the dithionite titration also results in the loss of flavin fluorescence.

As shown in Figure 2 anaerobic NADH titration of R303M Npx also occurs in two distinct phases; the first requires 1 equiv of reductant/FAD and results in an EH_2 intermediate indistinguishable from that observed with dithionite, both in terms of its absorbance spectrum and enhanced fluorescence. The small increase in long-wavelength absorbance beyond 500 nm could be consistent with a very weak Cys42-S^- → FAD charge-transfer interaction and is similar in intensity to that seen with 1 equiv of dithionite/FAD. More surprisingly, titration of this EH_2 form with an additional 1.3 equiv of NADH/FAD leads directly to complete flavin reduction; this process results in the appearance of a stable EH_4·NAD^+ complex as indicated by the intense charge-transfer band centered at 765 nm. Similar redox behavior has been observed before with Npx, but only in the C42S, C42A, and L40C mutants which lack the Cys42-SOH center (*7*, *11*). NADH titration of the wild-type Npx EH_2 form does lead to partial A450 bleaching as well as an increase in 750 nm absorbance, but this has previously been attributed to quantitative formation of an EH_2·NADH complex (*10*). While this point will be considered in detail in Discussion, it is clear that the stoichiometric EH_4·NAD^+ complex formation observed with R303M Npx on addition of 2 equiv of NADH/FAD is much greater than the extent of any EH_2 reduction seen with wild-type Npx under identical conditions. To examine this unusual thermodynamic property of the R303M Npx EH_2 species further, a similar titration was carried out with AcPyADH ($E'^\circ = -248$ mV, or 72 mV higher than NADH; ref *21*). As shown in Figure 2, the AcPyADH titration also leads to the stoichiometric (1.9 equiv of AcPyADH/FAD) reduction of R303M E → EH_4·$AcPyAD^+$, despite the much higher potential for the free pyridine nucleotide. The absorbance maximum for the $AcPyAD^+$ complex is blue-shifted ∼25 nm (to 740 nm), and there is an ∼50% increase in ϵ740 (4500 M^{-1} cm^{-1}) compared to ϵ765 for the NAD^+ complex (3100 M^{-1} cm^{-1}). The EH_2 intermediate observed with 1 equiv of AcPyADH is spectrally identical to that seen with NADH, on the other hand.

Taken together, these results indicate that the redox potential for the R303M Npx EH_2/EH_4 couple, while it is not the only factor responsible for the altered behavior observed with pyridine nucleotides, may be increased significantly relative to that of wild-type Npx ($E'^\circ = -312$ mV for EH_2/EH_4; ref *10*). This was tested directly by measuring the EH_2/EH_4 potential for R303M Npx by dithionite titration in the presence of the reference dye phenosafranin ($E'^\circ = -252$ mV). Reductions of the reference dye and enzyme (EH_2 form) were monitored at 520 and 404 nm, respectively. Following this procedure, a redox potential of −261 mV was determined for the R303M Npx EH_2/EH_4 couple; the plot of log $[EH_2]/[EH_4]$ versus log$[dye_{ox}]/[dye_{red}]$ has a slope of 0.9. The EH_2/EH_4 potential for R303M Npx is thus 51 mV more positive than that for wild-type enzyme, which is generally consistent with the more facile reductions by NADH and AcPyADH. Still, other important factors such as the preferential binding of the oxidized pyridine nucleotide products to EH_4 must contribute significantly to this altered behavior. The dithionite titration data for R303M Npx also indicate that the potential for the EH_2/EH_4 couple must be at least 82 mV lower than that for reduction of E → EH_2; from this it follows that the potential for the Cys42-SOH/Cys42-SH couple is ≥−179 mV.

pK_a for Cys42-SH in R303M EH_2 Form. One explanation for the absence of a significant EH_2 charge-transfer band in R303M Npx would be a shift in the pK_a for Cys42-SH from the unusually low value of ≤4.5 found in the wild-type EH_2 form (at 25 °C; ref *12*) toward a more normal Cys-SH pK_a (*22*). Initial attempts to determine whether increasing pH led

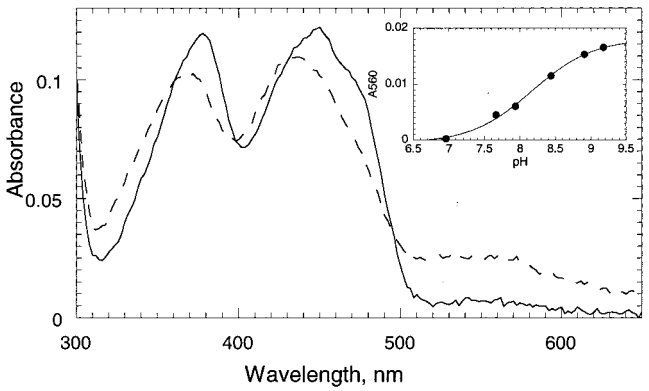

FIGURE 3: pH titration of R303M Npx EH_2 form. Enzyme was initially treated with 1 equiv of NADH/FAD to reduce any oxidized enzyme, and the air-stable EH_2 form was dialyzed as described in Figure 1. Spectra were recorded using the stopped-flow spectrophotometer, after mixing the R303M EH_2 form with concentrated buffers as described in Experimental Procedures. Spectra shown correspond to EH_2 (11.5 μM after mixing at 5 °C) at pH 7.0 (—) and 9.2 (- - -). Inset: Change in A560 versus pH. The titration curve yields a pK_a value of 8.2.

to enhanced EH_2 charge-transfer involved anaerobic tips to different buffers. While this method was successful in a limited sense, we modified this approach by performing pH-jump measurements with the R303M EH_2 form in the stopped-flow spectrophotometer at 5 °C. As shown in Figure 3, the pK_a determined for Cys42-SH from the absorbance change at 560 nm is 8.2. Although the replacement of His10 with Gln or Ala has no significant effect on the pK_a for Cys42-SH (*8*), substitution of Met for Arg303 results in a ≥3.7 unit increase. The much more favorable comparison between the mutant pK_a of 8.2 and the value of 9.1 reported by Tanford for Cys-SH (at 25 °C, as corrected for charged $-NH_3^+$ and $-CO_2^-$ groups; ref *22*) suggests that Arg303 plays a major role in increasing the acidity of Cys42-SH in the wild-type Npx EH_2 species.

Enzyme-Monitored Turnover and Steady-State Kinetics of R303M Npx. One concern prior to measuring initial rates of NADH oxidation with R303M Npx was based on the pronounced sensitivity of H10Q Npx to H_2O_2 inactivation, which results from peroxide oxidation of Cys42-SOH → Cys42-SO_2H/-SO_3H (*8*). As measured from the time-dependent loss of activity at several [H_2O_2]s, however, the second-order rate constant for H_2O_2 inactivation of R303M Npx is only 1.4 M^{-1} min^{-1} at 25 °C, or 5-fold less than the wild-type inactivation rate constant. In addition, changes in the visible absorbance spectrum of the mutant enzyme were observed during inactivation that resemble those seen with wild-type Npx (*23*), and there was an associated increase in flavin fluorescence.

When the R303M mutant was assayed under standard conditions with a recording spectrophotometer at 25 °C (pH 5.4, 0.16 mM NADH, 1−2 mM H_2O_2), initial rates corresponding to turnover numbers (as corrected for NADH oxidase activity) only 1−2% that of wild-type enzyme were obtained. These initial rates were linear for <1 min, and the NADH oxidase activity measured in the absence of H_2O_2, although unchanged from that of wild-type Npx, necessitated significant corrections. Under these conditions, however, it was determined that $K_m(H_2O_2)$ for R303M Npx was increased dramatically relative to wild-type enzyme. At pH 5.4, $K_m(H_2O_2) = 5.7$ mM [$k_{cat} = 8.2$ s^{-1}; $k_{cat}/K_m(H_2O_2) = 1.4 \times 10^3$ M^{-1} s^{-1}]; at 25 °C, these values contrast with $K_m(H_2O_2) = 0.13$ mM and $k_{cat} = 123$ s^{-1} at pH 5.5 [$k_{cat}/K_m(H_2O_2) = 9.5 \times 10^5$ M^{-1} s^{-1}] for wild-type Npx (*17*). The specificity constant for H_2O_2 is reduced by ~700-fold in the mutant. To allow direct comparisons with stopped-flow half-reaction measurements, these analyses were repeated in detail at 5 °C as described in the Experimental Procedures. The pH 7.0 steady-state kinetic parameters for R303M Npx are summarized in Table 2 with those for wild-type and H10Q enzymes.

Table 2: Steady-State Kinetic Parameters for Wild-Type, H10Q, and R303M Npxs at pH 7.0, 5 °C[a]

	k_{cat} (s^{-1})	K_m(NADH)	$K_m(H_2O_2)$	V_H/V_D
wild-type[b]	23.3	3 μM	14.1 μM	2.4
H10Q[b]	23.7	6.8 μM	0.69 mM	4.3
R303M	3.0	1 μM	6.4 mM	1.3

[a] Initial velocity measurements were made in 50 mM potassium phosphate, 0.1 M potassium acetate, pH 7.0, plus 0.5 mM EDTA. [b] Values from refs *8* and *10*.

When 21 μM R303M Npx (final concentration) was mixed in the stopped-flow spectrophotometer with 0.21 mM NADH and 40 mM H_2O_2, the enzyme rapidly approached a steady state (*16*, *24*) characterized by a predominant E-$FADH_2$·NAD^+ component, as monitored at 450 and 660 nm. NADH oxidation continued until this substrate was exhausted at ~5 s, although the A340 trace was not strictly linear. Integration of the A450 data set (*16*) gives $k_{cat} = 2$ s^{-1}, which agrees well with the steady-state value of 3 s^{-1} determined as described above. The spectral properties of the enzyme in turnover and the primary deuterium kinetic isotope effect were examined under similar conditions with (4*S*)-[4-^{1}H]- and (4*S*)-[4-^{2}H]NADH. When analyzed at 450 and 660 nm with 80 μM (4*S*)-[4-^{1}H]NADH and 14.6 μM enzyme in the presence of 40 mM H_2O_2 (Figure 4), the rapid approach to steady state corresponds to $k_{app} = 196$ s^{-1}, and the enzyme absorbance spectrum measured during steady-state turnover (λ_{max} ~770 nm with reduced A450) is very similar to that of the EH_4·NAD^+ complex observed in static titrations. When the same experiment is performed, but with 80 μM (4*S*)-[4-^{2}H]NADH, the approach to steady state is best analyzed as a biphasic process with rate constants of 222 and 37 s^{-1}.

Similar E-$FADH_2$·NAD^+ spectral intermediates are observed with both substrates, suggesting that the primary rate-limiting step in turnover is isotope-insensitive; we should add that since both EH_2' and EH_4 redox states are expected to exhibit similar absorbance spectra, specific identification of either form in steady-state turnover is not implied at this point.

Integration of the enzyme-monitored turnover data sets at 450 nm yields values for $k_{cat} = 2.3$ and 1.8 s^{-1} with (4*S*)-[4-^{1}H]- and (4*S*)-[4-^{2}H]NADH, respectively; V_H/V_D for R303M Npx is therefore 1.3, significantly less than the values of 2.3−4.3 determined for wild-type and His10 mutant enzymes (*8*). Both the V_H/V_D value and the predominance of an E-$FADH_2$·NAD^+ intermediate during steady-state turnover are consistent with a change in rate-limiting step for R303M Npx relative to the wild-type enzyme. The isotope-sensitive intramolecular hydride transfer within the E-FAD·NADH complex, which yields the EH_2 species as

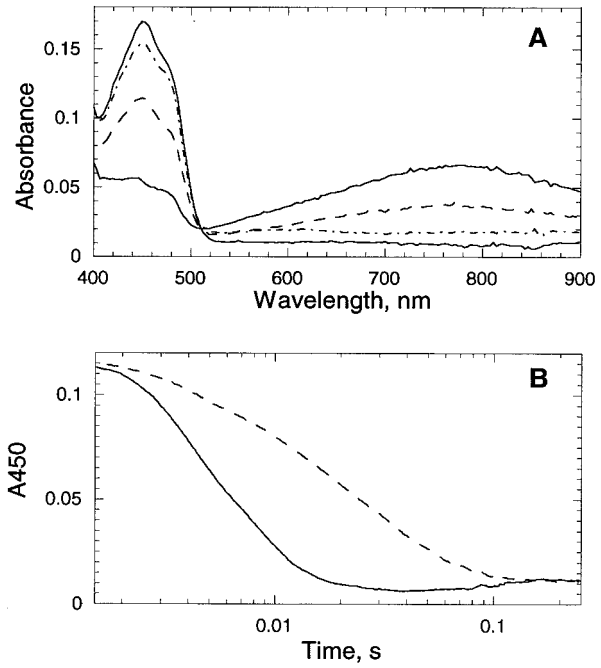

FIGURE 4: Enzyme-monitored turnover of R303M Npx with (4*S*)-[4-^{1}H]- and (4*S*)-[4-^{2}H]NADH. (A) Enzyme (14.6 μM after mixing, in 50 mM phosphate, 0.1 M acetate, pH 7.0, with 0.5 mM EDTA at 5 °C) was mixed anaerobically in the presence of 80 μM NADH and 40 mM H_2O_2, and the reaction was monitored by diode-array detection. Spectra correspond to the reaction mixture at 3.8 ms (- · -), 16.6 ms [steady state (—)], 2.7 s (— — —), and the fully oxidized enzyme 10 s after mixing (—). (B) A450 traces for the approach to steady state are given for the reaction desribed in [A (—)] and for the reaction in the presence of 80 μM (4*S*)-[4-^{2}H]-NADH (— — —).

observed with wild-type Npx (*10*), is not rate limiting with R303M Npx. To evaluate this conclusion further, enzyme-monitored turnover analyses were performed with R303M enzyme and AcPyADH. A preliminary experiment measuring initial rates of AcPyADH oxidation indicated that $k_{cat} = 0.1$ s^{-1} and $K_m(H_2O_2) = 0.1$ mM (at 66 μM AcPyADH; corrected for oxidase activity) at pH 7.0, 5 °C. The 30-fold decrease in k_{cat} and the longer reaction time required in enzyme-monitored turnover presented a technical problem due to the catalytic decomposition of H_2O_2 by the otherwise undetectable amounts of *E. coli* catalase present in the R303M Npx preparation. It has been shown previously, however, that azide can be used to inhibit this catalase activity without effect on Npx (*10*). When 30.3 μM R303M Npx (final concentration) was mixed with 0.14 mM AcPyADH and 2 mM H_2O_2 in the presence of 0.2 mM azide, the spectral course of turnover proceeded as given in Figure 5. Unlike NADH oxidation traces at 340 nm in similar experiments, AcPyADH oxidation led to A364 traces that yielded linear rates for ~10 s; the corresponding turnover number of 0.1 s^{-1} agrees very well with that from the preliminary determination described above. As with (4*S*)-[4-^{2}H]NADH, two rate constants of 158 and 41 s^{-1} were required to describe the approach to steady state with AcPyADH at both 450 and 660 nm. An E-FADH$_2$·AcPyAD$^+$ complex ($\lambda_{max} = 755$ nm) dominates the spectrum of the enzyme in steady-state turnover, suggesting that a similar rate-limiting step applies for both NADH and AcPyADH; the magnitude of this rate constant seems, however, to be sensitive to the bound pyridine nucleotide.

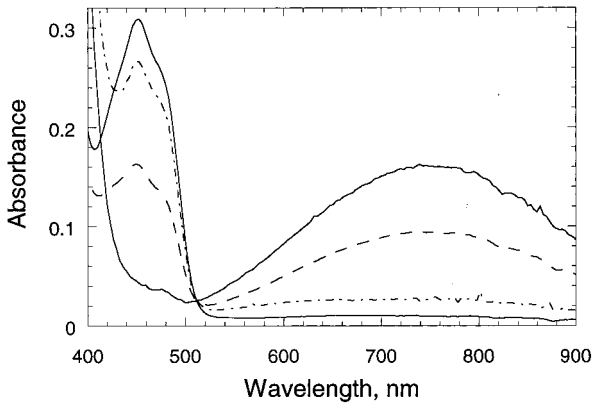

FIGURE 5: Enzyme-monitored turnover of R303M Npx with AcPyADH. Enzyme (30.3 μM after mixing, in the standard pH 7.0 phosphate/acetate buffer at 5 °C) was mixed anaerobically in the presence of 0.14 mM AcPyADH and 2 mM H_2O_2, with 0.2 mM azide present to inhibit catalase, and the reaction was monitored by diode-array detection. Spectra correspond to the reaction mixture at 1.2 ms (- · -), 0.25 s [steady state (—)], 29.7 s (— — —), and the fully oxidized enzyme 49.6 s after mixing (—).

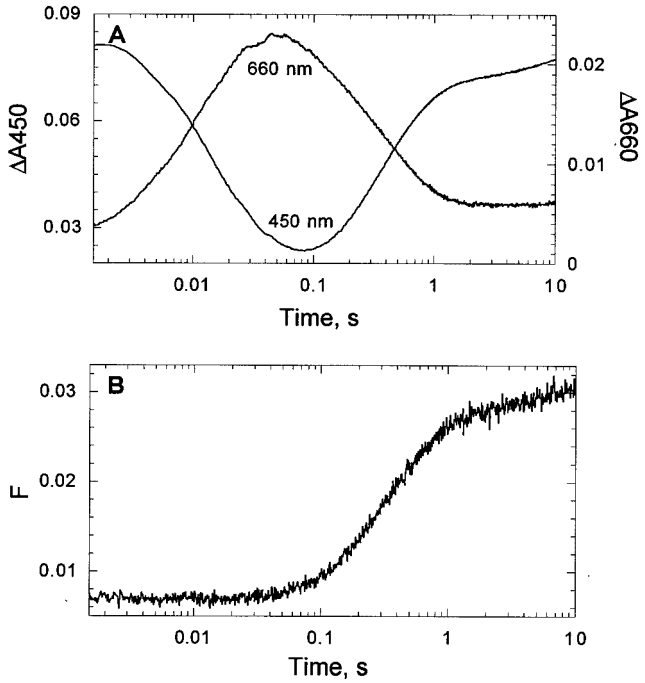

FIGURE 6: Stopped-flow analysis of the NADH reduction of R303M Npx E → EH$_2$. 9.7 μM oxidized enzyme (final concentration, in the standard pH 7.0 phosphate/acetate buffer at 5 °C) was mixed anaerobically with 9 μM NADH, and the reaction was monitored in the stopped-flow spectrophotometer (A) at 450 and 660 nm, and (B) at fluorescence emission wavelengths > 510 nm ($\lambda^{EX} = 450$ nm).

Reduction of R303M E → EH$_2$. The observation of an E-FADH$_2$·NAD$^+$ complex during steady-state turnover suggests that either intramolecular electron transfer from FADH$_2$ → Cys42-SOH (EH$_2'$ → EH$_2$) or the reoxidation of EH$_4$ with H_2O_2 (EH$_4$ → EH$_2$) is a component of the rate-limiting step with the R303M mutant. To examine the first possibility, the spectral and kinetic properties of the reduction of E → EH$_2$ with 0.9 equiv of NADH were examined. Figure 6 gives the result of an experiment in which the changes in absorbance at 450 and 660 nm were followed along with fluorescence ($\lambda^{EX} = 450$ nm, $\lambda^{EM} > 510$ nm) at 9.7 μM enzyme. The reaction is clearly biphasic to at least 1 s,

exhibiting a decrease in A450 (a lag in the fluorescence trace) followed by an increase in both A450 and fluorescence. Careful analysis reveals that four rate constants are required to interpret the full 10 s traces at both 450 and 660 nm. The decrease in A450 is biphasic, with rate constants of 77 and 22 s^{-1}. The major component of the A450 increase corresponds to $k = 2.7\ s^{-1}$ ($\sim k_{cat}$), while the slow phase ($k_{slow} = 0.1\ s^{-1}$) is not catalytically competent. This noncatalytic component accounts for about 20% of the total increase in A450 and is consistently seen in the fluorescence traces as well, as EH_2 is formed. The fluorescence data also give $k = 3\ s^{-1}$ ($\sim k_{cat}$) for the third phase in reduction of E → EH_2, which accounts for over 80% of the total fluorescence increase. This increase in fluorescence and the regain of A450, both at 2.7−3 s^{-1}, provide strong evidence for the transient formation of an EH_2'·NAD^+ species on reaction of R303M Npx with stoichiometric NADH. The subsequent intramolecular electron-transfer step corresponds to the conversion of EH_2'·NAD^+ → EH_2 and appears to be rate limiting in turnover as well.

In a parallel experiment the primary deuterium kinetic isotope effect on the reduction of E → EH_2 was investigated. The data set obtained with 0.9 equiv of (4*S*)-[4-^{1}H]NADH (14.6 μM enzyme) gives rate constants of 84, 24, and 2.6 s^{-1} for the reaction sequence at both 450 and 660 nm as described above; analysis of the noncatalytic component gives $k_{slow} = 0.2\ s^{-1}$. With 0.9 equiv of (4*S*)-[4-^{2}H]NADH a very similar reaction sequence is observed, but with rate constants of 46, 25, and 2.4 s^{-1} for the three catalytically competent phases. While the event attributed to reduction of E → EH_2' is isotope-sensitive ($k_H/k_D = 1.8$), the intramolecular electron-transfer step (EH_2' → EH_2; $k_H/k_D = 1.1$) is not. These results fully support the interpretation that the major component of the decrease in A450 (85% of the total amplitude change) observed at 84 s^{-1} with NADH is due to flavin reduction, and that the rate-limiting step in turnover is the subsequent transfer of electrons to Cys42-SOH at 2.6 s^{-1}. The diode-array data set obtained with NADH was then analyzed in conjunction with the rate constants determined from these single-wavelength measurements in order to calculate the absorbance spectra of the two catalytic intermediates. These are shown in Figure 7, and both spectra are indicative of E-$FADH_2$·NAD^+ complexes. These spectral and kinetic results are consistent with the overall scheme.

$$\mathrm{E} + \mathrm{NADH} \xrightarrow{84\ s^{-1}} (\mathrm{EH_2'}\cdot\mathrm{NAD^+})^* \xrightarrow{24\ s^{-1}} \mathrm{EH_2'}\cdot\mathrm{NAD^+} \xrightarrow{2.6\ s^{-1}} \mathrm{EH_2} + \mathrm{NAD^+} + \mathrm{H_2O}$$

The chemical distinction between (EH_2'·NAD^+)* and EH_2'·NAD^+ forms is not clear at present, but it does not involve either further reduction to EH_4, dissociation of NAD^+, or any slower reducing component of oxidized enzyme; there is no kinetic isotope effect on the conversion of (EH_2'·NAD^+)* → EH_2'·NAD^+, and there is only a slight decrease in ϵ775 during this step. In addition, both forms are essentially nonfluorescent.

As described above, k_{cat} for R303M Npx with AcPyADH is only 0.1 s^{-1}, or 30-fold less than with the natural substrate. The finding that the intramolecular transfer of electrons from

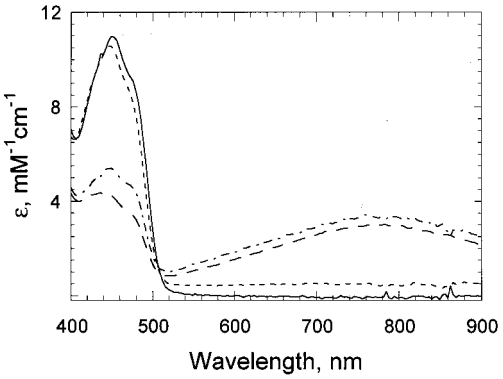

FIGURE 7: Calculated absorption spectra for intermediates B and C in the NADH reduction of R303M Npx E → EH_2. The reduction of E → EH_2 was analyzed in an experiment very similar to that described in Figure 6, but with 14.6 μM R303M Npx and 12.3 μM NADH. The entire 10 s, 100 spectrum data set from this diode-array experiment was analyzed as described in the Experimental Procedures and Results, using the rate constants for the three-step model described in the text. The spectrum shown for the starting oxidized enzyme (—) is taken directly from the diode-array data set. Additional spectra shown were calculated for intermediate B (- · -), intermediate C (— — —), and the final EH_2 form (- - -).

$FADH_2$ → Cys42-SOH is rate limiting with NADH was taken to suggest that this process might be sensitive to the nature of the pyridine nucleotide bound to EH_2'. When R303M Npx was reacted with 0.7 equiv of AcPyADH/FAD an EH_2'·$AcPyAD^+$ spectral intermediate very similar to that observed in steady-state turnover ($\lambda_{max} = 745$ nm) appears; this species is converted to EH_2 in a biphasic process with rate constants of 0.2 and 0.05 s^{-1}. It therefore appears that the rate-limiting intramolecular electron transfer is slowed significantly within the $AcPyAD^+$ complex, as compared to the rate constant of 2.6−2.7 s^{-1} measured with NADH. Furthermore, both rate constants measured on conversion of EH_2'·$AcPyAD^+$ → EH_2 differ by only 2-fold from k_{cat} with AcPyADH and could represent catalytic steps.

Reduction of R303M E → EH_4·NAD^+. When the reduction of R303M Npx with 5.2 equiv of NADH (76 μM final concentration) was monitored by diode-array detection, the observed rate constant for formation of the EH_2'·NAD^+ intermediate was increased to about 240 s^{-1}. A well-resolved slow phase with a rate constant of 4−5 s^{-1} ($\sim k_{cat}$ of 3 s^{-1}) led to the final EH_4·NAD^+ species, as limited presumably by the conversion of EH_2'·NAD^+ → EH_2. Further support for this interpretation comes from analysis of the reaction of the preformed R303M EH_2 intermediate with 5 equiv of NADH; in this case monophasic flavin reduction occurs with a k_{obs} value of about 280 s^{-1} and yields the EH_4·NAD^+ complex directly.

When the reaction of R303M Npx was analyzed with 5.2 equiv of (4*S*)-[4-^{2}H]NADH the two-electron reduction of EH_2'·NAD^+ → EH_4·NAD^+ was again limited by the formation of EH_2 at 4.1 s^{-1}; there is no isotope effect on this step ($k_H/k_D = 1.1$). As expected, however, the k_{obs} value for EH_2'·NAD^+ formation was isotope-sensitive. When the entire diode-array data set of 400 spectra was analyzed with the kinetic scheme,

$$\mathrm{A} \xrightarrow{53\ s^{-1}} \mathrm{EH_2'}\cdot\mathrm{NAD^+} \xrightarrow{4.1\ s^{-1}} \mathrm{EH_2} + \mathrm{NAD^+} + \mathrm{H_2O}$$

$$\mathrm{EH_2} + \mathrm{NADD} \xrightarrow{\gg 4.1\ s^{-1}} \mathrm{EH_4}\cdot\mathrm{NAD^+}$$

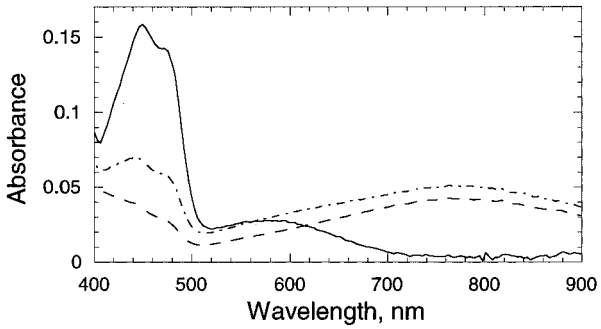

FIGURE 8: Calculated absorption spectra for intermediates in the reduction of R303M Npx E → EH_4·NAD^+ with (4*S*)-[4-^{2}H]NADH. The reduction of 14.6 μM oxidized enzyme with 75.5 μM (4*S*)-[4-^{2}H]NADH (final concentrations) was analyzed under anaerobic conditions very similar to those described for Figure 7. The data set of 400 diode-array spectra was used as described in both the Experimental Procedures and Results to calculate the absorption spectra for species A (—), intermediate B (- · -), and for the final EH_4·NAD^+ form (— — —). The kinetic scheme used in this analysis is presented in the text.

the calculated dead-time absorbance spectrum for species A (Figure 8) is clearly that of the R303M E·NADD complex, with an oxidized $\lambda_{max} = 449$ nm, a resolved shoulder at 471 nm, and a strong NADD → FAD charge-transfer band centered at 580 nm. The E·NADH complex of wild-type Npx, for example, has an oxidized λ_{max} of 450 nm, with a strong shoulder at 468 nm and a charge-transfer band centered at 560 nm (*10*).

Catalytic H_2O_2 Reactivity of R303M Npx. The reoxidation of the R303M EH_4·NAD^+ complex formally requires the reduction of 2 equiv of H_2O_2 per $FADH_2$,

$$EH_4{\cdot}NAD^+ + H_2O_2 \rightarrow EH_2'{\cdot}NAD^+ + H_2O$$

$$EH_2'{\cdot}NAD^+ \rightarrow EH_2 + NAD^+ + H_2O$$

$$EH_2 + H_2O_2 \rightarrow E + H_2O$$

However, we have also shown that the R303M EH_2 species is rapidly reduced to EH_4·NAD^+ in the presence of excess NADH; under standard assay conditions, with both substrates present at saturating concentrations [and in consideration of the $K_m(H_2O_2)$ value of 6.4 mM for this mutant], the extent of direct EH_2 participation in H_2O_2 reduction will depend on the relative rates of NADH reduction versus H_2O_2 oxidation. Given the instability observed with the mutant EH_2 form at higher pH values, we analyzed the reaction of 9.2 μM EH_2 with H_2O_2 by fluorescence at pH 7.0, 5 °C. Data averaged from 6 to 8 individual traces at each of several [H_2O_2]s ranging from 0.1 to 50 mM were biphasic, but k_{fast} represented almost 90% of the total ΔF throughout the [H_2O_2] range. A double-reciprocal plot of k_{fast} versus [H_2O_2] (*25*) yielded values for $K_d(H_2O_2)$ and k_{ox} of 2.5 mM and 310 s^{-1}, respectively,

$$EH_2 + H_2O_2 \overset{K_d = 2.5\ mM}{\rightleftharpoons} EH_2{\cdot}H_2O_2 \xrightarrow{310\ s^{-1}} E + H_2O$$

Crystal Structure of R303M Npx. The Ramachandran plot of the mutant structure is very similar to that of the native Cys42-SOH form of wild-type Npx (*3*, *18*). A single residue, Phe332, is found in the disallowed region; this residue occupies position $i + 1$ of a type II′ turn where glycine is usually required (*4*, *18*). The final R303M Npx model meets the geometric criteria applied with the program PROCHECK (*26*), and the rms deviations in bond lengths and angles are given in Table 1 along with the mean coordinate error. Both the latter value and the overall *B*-factor (0.25 Å and 39 Å^2, respectively) are higher than observed in the wild-type structure (0.15 Å and 20.7 Å^2; ref *18*), suggesting a greater degree of inherent disorder in the R303M mutant. Superimposition of the two structures reveals, however, that the mutation does not give rise to any domain movements or rearrangements; the overall tertiary structures remain very similar.

To visualize the differences in active-site structures for the wild-type and R303M Npxs, the C_α coordinates for the two proteins were superimposed using the least-squares method of Kabsch (*27*). As shown in Figure 9, the mutant structure confirms the presence of Met303, and Cys42-SOH is stabilized as a result of the cryogenic conditions employed in data collection. As Arg303 in wild-type Npx interacts with both His10 and Glu14, we first analyzed the environment of Met303. The closest approach of any Met303 side chain atom to either His10 $N_{\delta 1}$ or Glu14 $O_{\epsilon 1}$ is 3.8 Å, and the position of Met303 C_ϵ is displaced 3.0 Å from its N_ϵ equivalent in the Arg303 side chain. Similarly, there are no interactions between Met303 and Tyr60. In view of the potential disruption of the domain zipper described by Stehle et al. (*4*), a water molecule (Wat131) assumes the role of linking His10 $N_{\delta 1}$ (2.8 Å) and Glu14 $O_{\epsilon 1}$ (3.0 Å); this water is displaced by Arg303 in the wild-type structure. The loss of Arg303 does induce compensating changes in the side-chain conformations of Glu14 and Arg307 involving displacements of 0.7−1.0 Å in the respective $-O_{\epsilon 2}$ and $-N_{\eta 2}$ positions, but the salt bridge joining these two residues is maintained. There is almost no change in the orientation of the His10 side chain in the R303M mutant.

In view of the somewhat dramatic functional changes introduced by the R303M mutation, it should be emphasized that the 2.1 Å structure of wild-type Npx indicates that no element of the Arg303 guanidinium moiety is located within 7 Å of the Cyo42-SO function.[3] Nonetheless, there is a dramatic change in the Cyo42 side-chain conformation in the mutant relative to wild-type Npx. Even taking into consideration the greater degree of inherent disorder indicated for this mutant structure and the larger rms coordinate error, the displacements for Cyo42 S_γ and O_δ are 0.9 and 1.6 Å, respectively. As opposed to the essentially parallel arrangement indicated for the Cyo42 side chain and the FAD isoalloxazine in wild-type Npx (*3*, *18*), the Cyo42-SO function of the mutant adopts an "out" conformation that appears to involve a major rotation of the C_β-S_γ bond. This positions Cyo42 O_δ further from the isoalloxazine ring; while the distances to FAD C(10a), N(1), and C(4a) in wild-type Npx are 3.3−3.5 Å, Cyo42 O_δ is 4.0−4.5 Å from these loci in the mutant. As a consequence the SO oxygen is in a position to form hydrogen bonds with FAD O2′ (2.9 Å) and His10 $N_{\epsilon 2}$ (3.2 Å) as well as Cyo42 N (2.9 Å). The accompanying slight rotation about the C_α−C_β bond also has the effect of bringing Cys42 S_γ closer to FAD C(4a), C(10a), and N(5) (now separated by 3.1−3.5 Å) and other elements of the flavin redox center.

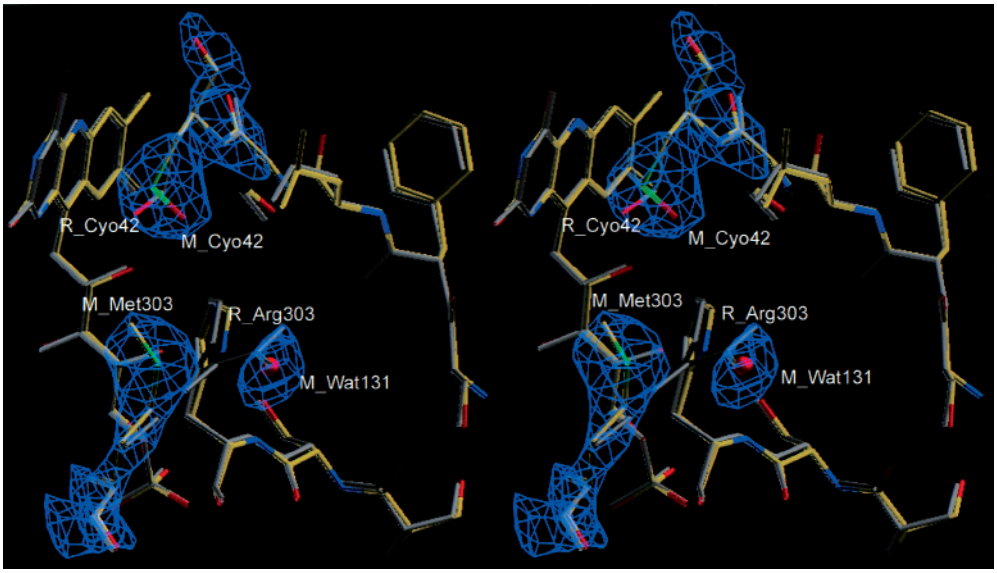

FIGURE 9: Stereoview of the superimposed active sites of wild-type (R_-prefix; in gray except for Cyo42 O_δ, in red) and R303M mutant (M_-prefix; colored according to atom type) peroxidases. Also shown is the σ_A-weighted $2|F_o| - |F_c|$ annealed omit map, contoured at 2σ, with 3.5 Å spherical omitted regions centered at residues 42 and 303 (Wat131 is included within the region omitted around residue 303). The electron densities clearly indicate the positions of the omitted residues and active-site water. Residues given without labels correspond to the active-site segments Ser8-Ser9-His10, Ser38-Phe39-Leu40-Ser41-, and the FMN portion of FAD.

DISCUSSION

Rate-Limiting Step in Catalysis is Changed in R303M Npx. The catalytic mechanism proposed for wild-type Npx (*10*) on the basis of combined steady-state and stopped-flow kinetic analyses consists of a pre-steady-state priming step in which oxidized enzyme is reduced with 1 equiv of NADH; the resulting EH_2 species is a central catalytic intermediate,

$$EH_2 + NADH \xrightarrow{(4-8) \times 10^6\ M^{-1}\ s^{-1}} EH_2{\cdot}NADH^*$$

$$EH_2{\cdot}NADH^* + H_2O_2 \xrightarrow{(2-3) \times 10^6\ M^{-1}\ s^{-1}} E{\cdot}NADH + H_2O$$

$$E{\cdot}NADH + H^+ \xrightarrow{25\ s^{-1}} EH_2{\cdot}NAD^+ + H_2O$$

$$EH_2{\cdot}NAD^+ \xrightarrow{250\ s^{-1}} EH_2 + NAD^+$$

The E·NADH complex was identified by diode-array analyses of the enzyme during steady-state turnover; its spectral properties are very similar to those of the E(Cys42-SO_3H)·NADH complex of Npx (*23*) as well as the NADPH complexes described for C47S (*28*) and oxidized EHR(Cys63-SO_3H; ref *29*) forms of *E. coli* and yeast GR, respectively. Stopped-flow analysis did not identify any discrete E-$FADH_2$ intermediate with wild-type Npx in either reductive half-reaction or enzyme-monitored turnover experiments, and a primary deuterium isotope effect of 3.0 was measured on the conversion of E·NADH → EH_2. This hydride transfer step is essentially rate limiting in turnover and accounts almost quantitatively for the pH dependence of k_{cat}, which exhibits an acidic optimum but decreases sharply above pH 6.5, with an apparent pK_a of 6.9 for some activity-limiting ionization within the E·NADH complex. This pK_a does not correspond to the active-site His10, since His10 mutants exhibit essentially identical k_{cat} values and k_{cat} versus pH profiles as wild-type Npx (*8*).

In contrast to the E·NADH intermediate which dominates the steady-state turnover spectrum of wild-type Npx, the R303M mutant provides direct evidence for an E-$FADH_2$ intermediate in the transfer of electrons from NADH to Cys42-SOH. The corresponding $EH_2'{\cdot}NAD^+$ complex is easily distinguished by its spectral properties (Figure 4A), and integration of enzyme-monitored turnover traces at 450 nm gives a value for k_{cat} (2−2.3 s^{-1}) very close to that determined (3 s^{-1}) from initial rates of NADH oxidation. Furthermore, we have shown that this conversion of $EH_2'{\cdot}NAD^+$ → EH_2 is the rate-limiting step in turnover, as demonstrated in reductive half-reaction analyses with 0.9 equiv of NADH; these experiments give values of 2.4−3 s^{-1} for the corresponding rate constant (Figures 6 and 7). Using (4*S*)-[4-^{2}H]NADH we have shown that there is no primary deuterium isotope effect on this step, nor is there an isotope effect on turnover with R303M Npx. These observations, taken together with the spectral properties of the enzyme in steady-state turnover, clearly indicate that the E-$FADH_2$ species is a true intermediate in Cys42-SOH reduction and that the R303M mutation introduces a change in the rate-limiting step in catalysis.

By investigating the reduction of R303M Npx with a 5-fold excess of deuterated substrate (Figure 8), we were also able to demonstrate the dead-time formation of an E·NADD complex similar to that observed with the wild-type enzyme and NADH. Still, under otherwise identical conditions, the observed rate constant for hydride transfer to FAD (46 s^{-1}) within the R303M E-FAD·NADD complex is faster than that for the comparable conversion of wild-type E-FAD·NADH → EH_2 (23 s^{-1}). Taken together, the spectral and kinetic results provide the following mechanistic scheme for the stoichiometric reduction of R303M Npx,

$$E + NADH \overset{K_{NADH}}{\rightleftharpoons} E{\cdot}NADH \xrightarrow{k_{red}} (EH_2'{\cdot}NAD^+)^*$$

$$(EH_2'{\cdot}NAD^+)^* \xrightarrow{24\ s^{-1}} EH_2'{\cdot}NAD^+$$

$$EH_2'{\cdot}NAD^+ \xrightarrow{2.4-3\ s^{-1}} EH_2 + NAD^+$$

In the presence of a 5-fold excess of NADH k_{obs} is ~240 s^{-1} for the reduction of E → $(EH_2'{\cdot}NAD^+)$*, and the EH_2 species is rapidly reduced to the stable $EH_4{\cdot}NAD^+$ form with an observed rate constant approaching 300 s^{-1}. This $EH_4{\cdot}NAD^+$ species is identical to the final R303M Npx form obtained in anaerobic titrations with 2 equiv of NADH/FAD (Figure 2A). Stopped-flow fluorescence analyses indicate that the kinetic mechanism for the EH_2 reaction with H_2O_2 differs significantly from that with wild-type Npx, consistent with the dramatic increase in $K_m(H_2O_2)$ of nearly 500-fold observed on substitution of Met for Arg303. The irreversible second-order reaction demonstrated for the wild-type enzyme is replaced by a two-step mechanism,

$$EH_2 + H_2O_2 \overset{K_{H_2O_2}}{\rightleftharpoons} EH_2{\cdot}H_2O_2$$

$$EH_2{\cdot}H_2O_2 \xrightarrow{k_{ox}} E + H_2O$$

where $K_{H_2O_2}$ = 2.5 mM (approaching the K_m value of 6.4 mM) and k_{ox} = 310 s^{-1}. A major factor in the mM K_d for the rapid equilibrium step derives from the increased pK_a value for Cys42-SH; at pH 7.0 only 6% of the R303M EH_2 form carries the Cys42-thiolate essential for peroxide reduction.

$EH_4{\cdot}NAD^+$ Redox States in Wild-Type and R303M Npxs. An additional aspect of the wild-type Npx mechanism (*10*) involves the distinction between the $EH_2{\cdot}NADH$* catalytic intermediate and the static $EH_2{\cdot}NADH$ species identified in spectral titrations. The rate constant for conversion of $EH_2{\cdot}NADH^*$ → $EH_2{\cdot}NADH$ (10 s^{-1}) is less than k_{cat} (23 s^{-1}), indicating that the static species is not catalytically competent. Furthermore, this conversion (in the presence of 5 equiv of NADH/FAD) corresponds to decreases in both A450 and A570, suggestive of a significant E-FAD → E-$FADH_2$ component. Static titrations revealed, however, that the conversions of EH_2 → $EH_2{\cdot}NADH$ and $EH_2{\cdot}AcPyADH$ complexes exhibited isosbestic behavior throughout, and the same $EH_2{\cdot}NADH$ complex was formed on titration of the Npx EH_4 form with NAD^+. More recently we have shown[4] that back-titration of the static $EH_2{\cdot}NADH$ complex with ferricyanide also leads to stoichiometric conversion to EH_2 [2 equiv of $Fe(CN)_6^{-3}$ per FAD] in a similar isosbestic fashion. On the basis of these observations we concluded that these EH_2 complexes did not reflect significant EH_4 contributions. We also demonstrated (*10*) that the static $EH_2{\cdot}NADH$ complex only very slowly approached a catalytically competent steady state, with k_{app} = 4−5 s^{-1} versus 480−520 s^{-1} for the E and EH_2 forms, and its direct reoxidation by H_2O_2 was slower than turnover.

The static $EH_2{\cdot}NADH$ complex is, however, reactive toward oxygen (*12*); in contrast to the EH_2 form, this indicates the presence of some equilibrium E-$FADH_2$ component. Recent titrations of wild-type Npx[4] with NADH in CHES buffer, pH 8.8, even indicate that the enzyme can be reduced completely to the EH_4 form with a total of 2 equiv of NADH/FAD; 2 equiv of $Fe(CN)_6^{-3}$ quantitatively reoxidizes EH_4 → EH_2. Considering the present titration data with R303M Npx and both NADH and AcPyADH, which demonstrate direct formation of the EH_4 complex with the respective pyridine nucleotide product (Figure 2), the long-wavelength λ_{max} values of 765 and 740 nm for these reduced enzyme forms support the revised interpretation that the $EH_2{\cdot}NADH$ and AcPyADH complexes with wild-type Npx at pH 7.0 also contain significant $EH_4{\cdot}NAD^+$ and $EH_4{\cdot}AcPyAD^+$ components at equilibrium. In particular, the difference spectra beyond 500 nm accompanying these wild-type EH_2 titrations (*10*) can now be interpreted as the combination of two effects: NADH (or AcPyADH) enhancement of EH_2 charge-transfer over the range 500−650 nm, and E-$FADH_2{\cdot}NAD^+$ (or $AcPyAD^+$) charge-transfer absorbance from 650 to 800 nm. The effect of NADPH on EH_2 thiolate→FAD charge-transfer absorbance has previously been described by Rietveld et al. (*28*) with GR, and the observation of an E-$FADH_2$ → NAD^+ charge-transfer band at 740 nm in the Npx C42S mutant (*11*) establishes the basis for the latter spectral component in both wild-type and R303M Npxs. In the present work we have also established that substitution of Met for Arg303 in Npx leads to a 51 mV increase (to −261 mV) in E'° for the FAD/$FADH_2$ couple. In the presence of one equiv of AcPyADH (E'° = −248 mV), however, the R303M EH_2 form is quantitatively reduced to the $EH_4{\cdot}AcPyAD^+$ species (Figure 2B). Rietveld et al. (*28*) have also suggested, on the basis of studies with *E. coli* GR Cys42 and Cys47 mutants, that the differential binding of pyridine nucleotide to E-FAD and E-$FADH_2$ forms can have a strong influence on the corresponding flavin potential. Previous studies with the wild-type Npx $EH_2{\cdot}AcPyADH$ complex (*10*), which were interpreted in light of the free solution potential for the pyridine nucleotide, were subject to this effect as well. In the context of the present analysis, we would also conclude that the conversion of $EH_2{\cdot}NADH^*$ → $EH_2{\cdot}NADH$ measured at 570 nm with wild-type Npx is actually attributable to formation of the small amount of $EH_4{\cdot}NAD^+$ component which is present at equilibrium.

Equilibrium Properties of the Cys42-SOH/-SH Redox Center Are Altered in R303M Npx. The results with R303M Npx can also be compared with those of other Npx mutants in which Cys42 has either been replaced (C42S, C42A; ref *11*) or oxidized to an active-site disulfide (L40C; ref *7*). While oxidized R303M Npx retains only 1−2% of the fluorescence of free FAD, the fluorescence of these mutants (22% of free FAD with L40C) compares favorably with that of the R303M EH_2 form. Visser et al. (*30*) have concluded that Cys42-SOH is probably responsible for the static fluorescence quenching observed in wild-type Npx; based on earlier studies with 8α-sulfur-linked flavin analogues in hydrogen-bonding solvents (*31*), it was shown that the observed fluorescence quenching was due to an interaction of the nonbonding electrons of Cys S_γ with the isoalloxazine ring and the solvent. The increase in fluorescence observed on reduction of R303M Npx to its EH_2 form (Cys42-SOH → Cys42-SH; Figures 1 and 6B) may therefore reflect a change in the S_γ hydrogen-bonding pattern and/or a deviation from the rigid steric requirement intrinsic to the sulfur quenching in oxidized R303M. Another feature shared by the C42S, C42A, L40C, and R303M mutants is the fact that all are reduced directly with NADH (1 equiv/FAD for Cys42 and L40C mutants and 2 equiv/FAD for R303M) to the

[4] H. A. van den Burg, D. Parsonage, and A. Claiborne, unpublished results.

respective E-$FADH_2$·NAD^+ complexes; in part this reflects the increase in FAD/$FADH_2$ redox potential in each case, ranging from −261 mV for the EH_2 form of R303M to −197 mV for the oxidized form of C42A Npx. These dramatic shifts have previously been attributed (*11*) to the absence of the charge-transfer interaction with the electron-rich Cys42-thiolate in each case, and the finding in the present study that the Cys42-SH pK_a = 8.2 for the R303M EH_2 form (Figure 3) fully supports and extends that conclusion. In view of the documented participation of an E-$FADH_2$·NAD^+ intermediate in the catalytic cycle of R303M Npx, it is important to point out that similar intermediates were identified in enzyme-monitored turnover analyses of both C42S and L40C mutant enzymes, although the k_{cat} values in these cases are both ≤0.1 s^{-1}. It was also shown (*11*) that the C42S mutant was reduced by NADH under pseudo-first-order conditions at an observed rate constant of 280−305 s^{-1}, comparable to the k_{obs} values of ∼240−280 s^{-1} measured for flavin reduction with oxidized and EH_2 forms of R303M Npx. The $K_d(NAD^+)$ for C42S E-$FADH_2$ binding, however, is higher than for R303M, allowing the determination of k_{off} = 134 s^{-1} for NAD^+ release in the former case. We have similarly estimated the rate constant for NAD^+ release from the wild-type Npx EH_2 form at ≥250 s^{-1}; both values are much greater than the rate-limiting reduction of Cys42-SOH within the R303M EH_2'·NAD^+ intermediate. Further evidence that NAD^+ release follows the redox step comes from the fact that the bound pyridine nucleotide has a considerable effect on the rate of EH_2 formation. In a carefully monitored dithionite titration we measured a $t_{1/2}$ of 12.3 min for the conversion of EH_2' → EH_2 at 25 °C; at 5 °C, however, the conversion of EH_2'·NAD^+ → EH_2 is at least 3 orders of magnitude faster. Intramolecular electron transfer within the EH_2'·$AcPyAD^+$ complex is 10−20-fold slower than with bound NAD^+, again reflecting the effect of the pyridine nucleotide.

Mechanistic Considerations for $FADH_2$ → Cys42-SOH Electron Transfer in Npx. In several respects, our results with the R303M peroxidase resemble those reported by Rietveld et al. (*28*) for the *E. coli* GR H439A mutant. As with R303M Npx, a discrete GR E-$FADH_2$·$NADP^+$ intermediate was only observed in the reductive half-reaction of the H439A mutant, not with the wild-type enzyme. This was attributed to a 16-fold decrease in the rate constant for electron transfer from $FADH_2$ to the redox-active disulfide in the GR mutant; stabilization of the nascent Cys47-thiolate (equivalent to Npx Cys42) by the protonated His439′ was proposed to facilitate the process of disulfide reduction in wild-type GR. These observations are generally consistent with the fact that H439A GR exhibits k_{cat} <1% that of wild-type enzyme, where the limiting rate of EH_2 oxidation by GSSG appears to be 4−5 times faster than the rate of enzyme reduction by NADPH (490 and 110 s^{-1}, respectively, at 4 °C). Further support for this catalytically important interaction between His439′ and the Cys47 charge-transfer thiol was provided by Deonarain et al. (*32*), who demonstrated that the Cys47-SH pK_a in a C42A, H439A double mutant was increased to 7.7 from a value of 5.7 in the C42A single mutant. This 2-unit shift in pK_a, which is reflected in a significantly diminished EH_2 charge-transfer band at pH 7.0, is qualitatively similar to that seen in the R303M Npx EH_2 form, where the magnitude of the pK_a increase is ≥3.7 units (Figure 3).

As to the chemical mechanism of Npx Cys42-SOH reduction, we have previously considered the possibility of direct hydride transfer from $FADH_2$ N5 to the sulfur (*18*). Karplus and Schulz (*33*) suggested that a transient FADH C4a−S_γ Cys63 covalent adduct could be involved in the comparable process of GR disulfide reduction. Cys63 S_γ is 3.5 Å from FAD C4a, and the Cys58−Cys63 disulfide bond is in line with the proposed nucleophilic center, optimizing the geometric considerations for an S_N2 displacement. The fate of the FADH N5 hydrogen was not clear, however. Vanoni et al. (*34*) reported a primary deuterium kinetic isotope effect of 4.0 for the reduction of spinach GR E → EH_2 with (4*S*)-[4-^{2}H]NADH, but this was attributed to hydride transfer within the E·NADH complex; no discrete E-$FADH_2$ species was observed. The present study with R303M Npx clearly demonstrates the absence of an isotope effect on the $FADH_2$ reoxidation rate constant, as E → EH_2 with (4*S*)-[4-^{2}H]NADH. The FAD N5 and −O4α positions in Npx are not accessible to solvent (*35*), suggesting that solvent exchange with the $FADH_2$ N5 hydrogen (or deuterium) is likely to be very slow. These results are suggestive of a mechanistic alternative to direct hydride transfer from $FADH_2$ → Cys42-SOH, possibly involving a C4a-adduct such as that proposed by Karplus and Schulz (*33*). There are two other factors that must be considered along with these proposals; first, unlike the situation with wild-type Npx, Cys42-SOH is likely to be protonated in the resting, oxidized R303M enzyme. In addition, the crystal structure of the mutant shows that the orientation of the Cyo42 S_γ−O_δ bond, relative to the plane of the flavin, is changed rather dramatically (Figure 9). Both factors are likely to contribute significantly to the efficiency of electron transfer from $FADH_2$ to the Cys42-SOH redox center.

At a minimum, the presence of Arg303 in Npx certainly stabilizes the nascent Cys42-thiolate formed on reduction of E → EH_2, and this effect may be taken to account for a component of the thermodynamic stabilization of EH_2. Regardless of the specific mechanism involved, the transfer of electrons from $FADH_2$ → Cys42-SOH must involve a transition state with partial negative charge on Cys42 S_γ (*18*); stabilization of this charged transition state by Arg303 would also account for the much more rapid $FADH_2$ reoxidation rate with wild-type Npx ($k \gg 25$ s^{-1}) compared to the R303M mutant (k = 2.4−3 s^{-1}). Analysis of the recent 2.1 Å structure of the native wild-type enzyme,[3] however, demonstrates clearly that the closest approach between Cyo42 S_γ and the charged guanidinium moiety of Arg303 is 7.9 Å. In the absence of an unusual long-range electrostatic effect, it is tempting to suggest that this effect is mediated by the intervening His10; we have already shown, however, that His10 mutants of Npx retain strong EH_2 charge-transfer properties at pH 5.4 (*8*). It should also be pointed out that the 2.0 Å structure of the EH_2·NADH complex of human erythrocyte GR (*33*) shows that His467′ $N_{\epsilon 2}$ (equivalent to His439′ in the *E. coli* enzyme), although it is directly implicated in stabilization of the charge-transfer thiolate by the results of Deonarain et al. (*32*), is 4.7 Å from the charge-transfer Cys63 S_γ in the human enzyme. The effects of both the active-site His in GR and Arg303 in Npx on the respective Cys-SH pK_a values may be enhanced by the apolar

active-site microenvironments that apply in both cases. The structures of the wild-type Npx EH_2·NADH complex and oxidized His10 mutants have recently been solved[3] and should offer additional information on this apparent paradox.

ACKNOWLEDGMENT

We thank Dr. Derek Parsonage for guidance in the initial phase of this work and for helpful discussions.

REFERENCES

1. Dolin, M. I. (1957) *J. Biol. Chem. 225*, 557−573.
2. Claiborne, A., Crane, E. J., III, Parsonage, D., Yeh, J. I., Hol, W. G. J., and Vervoort, J. (1997) in *Flavins and Flavoproteins 1996* (Stevenson, K. J., Massey, V., and Williams, C. H., Jr., Eds.) pp 731−740, University of Calgary Press, Calgary, AB.
3. Claiborne, A., Yeh, J. I., Mallett, T. C., Luba, J., Crane, E. J., III, Charrier, V., and Parsonage, D. (1999) *Biochemistry 38*, 15407−15416.
4. Stehle, T., Ahmed, S. A., Claiborne, A., and Schulz, G. E. (1991) *J. Mol. Biol. 221*, 1325−1344.
5. Stehle, T., Claiborne, A., and Schulz, G. E. (1993) *Eur. J. Biochem. 211*, 221−226.
6. Mande, S. S., Parsonage, D., Claiborne, A., and Hol, W. G. J. (1995) *Biochemistry 34*, 6985−6992.
7. Miller, H., Mande, S. S., Parsonage, D., Sarfaty, S. H., Hol, W. G. J., and Claiborne, A. (1995) *Biochemistry 34*, 5180−5190.
8. Crane, E. J., III, Parsonage, D., and Claiborne, A. (1996) *Biochemistry 35*, 2380−2387.
9. Crane, E. J., III, Vervoort, J., and Claiborne, A. (1997) *Biochemistry 36*, 8611−8618.
10. Crane, E. J., III, Parsonage, D., Poole, L. B., and Claiborne, A. (1995) *Biochemistry 34*, 14114−14124.
11. Parsonage, D., and Claiborne, A. (1995) *Biochemistry 34*, 435−441.
12. Poole, L. B., and Claiborne, A. (1986) *J. Biol. Chem. 261*, 14525−14533.
13. Massey, V. (1991) in *Flavins and Flavoproteins 1990* (Curti, B., Ronchi, S., and Zanetti, G., Eds.) pp 59−66, Walter de Gruyter, New York.
14. Mallett, T. C., and Claiborne, A. (1998) *Biochemistry 37*, 8790−8802.
15. Charrier, V., Luba, J., Parsonage, D., and Claiborne, A. (2000) *Biochemistry 39*, 5035−5044.
16. Gibson, Q. H., Swoboda, B. E. P., and Massey, V. (1964) *J. Biol. Chem. 239*, 3927−3934.
17. Parsonage, D., Miller, H., Ross, R. P., and Claiborne, A. (1993) *J. Biol. Chem. 268*, 3161−3167.
18. Yeh, J. I., Claiborne, A., and Hol, W. G. J. (1996) *Biochemistry 35*, 9951−9957.
19. Otwinowski, Z., and Minor, W. (1997) *Methods Enzymol. 276*, 307−326.
20. Poole, L. B., and Claiborne, A. (1989) *J. Biol. Chem. 264*, 12322−12329.
21. Loach, P. A. (1976) in *Handbook of Biochemistry and Molecular Biology* (Fasman, G. D., Ed.) 3rd ed., Vol. I, pp 122−130, CRC Press, Boca Raton, FL.
22. Tanford, C. (1962) *Adv. Protein Chem. 17*, 69−165.
23. Poole, L. B., and Claiborne, A. (1989) *J. Biol. Chem. 264*, 12330−12338.
24. Gutfreund, H. (1972) *Enzymes: Physical Principles*, John Wiley & Sons, New York.
25. Strickland, S., Palmer, G., and Massey, V. (1975) *J. Biol. Chem. 250*, 4048−4052.
26. Laskowski, R. A., MacArthur, M. W., Moss, D. S., and Thornton, J. M. (1993) *J. Appl. Crystallogr. 26*, 283−291.
27. Kabsch, W. (1978) *Acta Crystallogr., Sect. A 34*, 827−828.
28. Rietveld, P., Arscott, L. D., Berry, A., Scrutton, N. S., Deonarain, M. P., Perham, R. N., and Williams, C. H., Jr. (1994) *Biochemistry 33*, 13888−13895.
29. Miller, H., and Claiborne, A. (1991) *J. Biol. Chem. 266*, 19342−19350.
30. Visser, A. J. W. G., van den Berg, P. A. W., Visser, N. V., van Hoek, A., van den Burg, H. A., Parsonage, D., and Claiborne, A. (1998) *J. Phys. Chem. B 102*, 10431−10439.
31. Falk, M. C., and McCormick, D. B. (1976) *Biochemistry 15*, 646−653.
32. Deonarain, M. P., Scrutton, N. S., Berry, A., and Perham, R. N. (1990) *Proc. R. Soc. London B 241*, 179−186.
33. Karplus, P. A., and Schulz, G. E. (1989) *J. Mol. Biol. 210*, 163−180.
34. Vanoni, M. A., Wong, K. K., Ballou, D. P., and Blanchard, J. S. (1990) *Biochemistry 29*, 5790−5796.
35. Ahmed, S. A., and Claiborne, A. (1992) *J. Biol. Chem. 267*, 3832−3840.

BI000553M